Published in final edited form as:
Electrophoresis. 2012 November ; 33(21): . doi:10.1002/elps.201200263.

Microfluidic Transport in Microdevices for Rare Cell Capture

James P. Smith, **Alexander C. Barbati**, **Steven M. Santana**, **Jason P. Gleghorn**[†], and **Brian J. Kirby**
Sibley School of Mechanical and Aerospace Engineering, Cornell University

Abstract

The isolation and capture of rare cells is a problem uniquely suited to microfluidic devices, in which geometries on the cellular length scale can be engineered and a wide range of chemical functionalizations can be implemented. The performance of such devices is primarily affected by the chemical interaction between the cell and the capture surface and the mechanics of cell–surface collision and adhesion. As rare cell capture technology has been summarized elsewhere [1], this article focuses on the fundamental adhesion and transport mechanisms in rare cell capture microdevices, and explores modern device design strategies in a transport context. The biorheology and engineering parameters of cell adhesion are defined; adhesion models and reaction kinetics briefly reviewed. Transport at the microscale, including diffusion and steric interactions that result in cell motion across streamlines, is discussed. The review concludes by discussing design strategies with a focus on leveraging the underlying transport phenomena to maximize device performance.

Keywords

cell adhesion; circulating tumor cell; microfluidic transport; rare cell capture

1 The rare cell adhesion problem

Capture of rare cells from complex samples is a long-standing goal of increasing importance. Microfluidic devices have demonstrated impressive advances in this area [1] because of the ability to customize geometry on length scales comparable to cell size, a wide range of chemical functionalizations suitable for microfluidic implementation, and the portability and inexpensiveness of microfluidic systems produced in quantity.

An important subset of rare cell capture devices use immunospecific surfaces for cell capture and enrich rare populations based on the specific nature of the interaction of cell antigens with antibody-functionalized or aptamer-functionalized surfaces. These devices have isolated CD4- and CD8-positive cells in blood of HIV patients [2], CD34-positive endothelial progenitor cells [3], and epithelial markers in circulating tumor cells (CTCs) of cancer patients [4–8].

The performance of rare cell capture devices is affected primarily by the specificity and affinity of the chemical interaction and the mechanics of cell-wall collision and adhesion. Modern immunocapture devices for rare cells use both chemical and fluid-dynamic optimization to maximize efficiency and purity of capture.

Correspondence: Dr. Brian J. Kirby, 238 Upson Hall, Cornell University, Ithaca, NY 14853, USA. kirby@cornell.edu Phone: +1-607-255-4379. Fax: +1-607-255-1222.
[†]Present affiliation: Department of Chemical and Biological Engineering, Princeton University

The authors have declared no conflicts of interest.

1.1 Surface markers

Capture based on surface markers has been influenced by the long history of flow cytometry for cell enumeration and characterization in complex samples, e.g., blood [9–12]. Many surface markers can be used to identify the lineage or function of the cell. These surface markers are also informed by immunotherapeutic approaches that seek to bind toxins, contrast agents, or energy transducers (e.g., gold nanoparticles) to specific cells [13–16].

Both physicochemical and biological concerns affect the importance of a cell marker. Physicochemically, the ideal surface marker has an identifiable extracellular domain for which antibodies or aptamers exist, is present at high density on cells of interest, is as long as possible, and is not enzymatically cleaved in the sample domain. Biologically, the ideal surface marker has a known function, is correlated specifically to a desired cell subpopulation, and is not regulated by mechanical forces experienced in microscale flow.

Some examples of common markers for cancer cells include epithelial adhesion molecules such as EpCAM [17, 18], mucins such as MUC1, MUC4, and MUC16 [19–22], and upregulated receptors such as the folate receptor, EGFR, VEGFR, and Her2/neu [23]. Other markers (e.g., PSMA) often have unknown function in the disease state but have well-established correlations with the desired organ [24] and have been used to isolate cancer populations [25]. Stem or progenitor cell characteristics associated with antigens such as VEGFR1, VEGFR2, CD34, CD38, CD44, and CD133 are also often deemed important, either because they identify tumorinitiating cells or because their existence highlights a population associated with angiogenesis and conversion from micro-metastases to macro-metastases [26].

1.2 Cell sizes and distributions

Blood is dominated numerically and volumetrically by erythrocytes (6–9 μm), thrombocytes (2– 3 μm), and leukocytes (8–14 μm) [27]. Although blood cell populations have reasonably tight size distributions, rare cells often have widely variable and dynamic sizes, as demonstrated for progenitor cells, fetal cells, and circulating tumor cells [28]. Size alone is insufficient to identify rare cells, but provides a distinguishing characteristic; for example, erythroblasts and circulating tumor cells are both large relative to most blood cells. A key confounding issue is that the rare cells of scientific interest are often heterogenous and dynamic; as they play a dynamic role in human development and disease, differentiation and adaptation often cause these cells to change in size with time and environment via exosomal shedding and other processes [29, 30] making the instantaneous distribution of sizes in the population relatively broad.

1.3 Impact of efficiency and purity on downstream measurements

Efficiency and purity are both important in rare cell capture applications. Considering the rare cell capture device as a sensor, these attributes can be thought of as the two axes on the receiver operating characteristic curve that characterizes the sensor, as shown in Figure 1. The *capture efficiency* defines the fraction of target cells that are captured by the device (the *true positive rate* or *sensitivity* in sensor parlance). The *capture purity* defines the fraction of captured cells that are target cells (one minus the *false positive rate* or *1 – specificity*).

Either efficiency, purity, or both may be important for a specific application. High efficiency enables the study of rare events, such as the capture of CTCs from whole blood, while low efficiency prohibits such studies. Flow cytometry, for example, is relatively ineffective at handling rare cell events because all cells are analyzed and finding a rare cell (e.g., a CTC) requires enormous analysis. High purity enables direct downstream analysis, whereas low

purity (i.e., enrichment rather than detection) requires an additional downstream step to identify the cells of interest.

The relative importance of purity depends on the the downstream analysis that follows rare cell capture. For capture techniques that use a downstream technique to identify false positives, the purity is of lesser importance and priority is placed on efficiency. The Veridex CellSearch device and predecessors [31, 32] are examples of low purity capture devices — immunostaining of $EpCAM^+$-enriched cells distinguishes circulating tumor cells from contaminating leukocytes, so the relatively low purity of $EpCAM^+$ enrichment does not inhibit CTC enumeration. In fact, rapid detection can obviate enrichment entirely [33]. Purity is also unimportant when looking for genetic markers specific to the target population and absent from contaminants, for example when looking for cancer-specific gene fusions in CTCs [34]. In contrast, techniques that proceed directly to downstream analysis (e.g., RNA analysis or epigenomic modifiction) require high purity.

Because purity and efficiency have different importance in different applications, the best measures of merit encompass both of these factors. A specific implementation is best characterized by its efficiency and purity, whereas a general approach is often best evaluated by plotting the ROC curve in efficiency–purity space where the position on the contour is a function of a critical parameter. For example, the capture of rare cells from blood can be plotted in efficiency–purity space as a function of mean flow velocity or flow rate, as shown in Figure 1. The area under this curve (i.e., AUC) gives a holistic evaluation of the quality of the measurement approach rather than a specific parametric value.

2 Engineering parameters that affect cell adhesion

Cell adhesion is governed by several parameters: the local shear stress, the immunospecificity, and biorheology. Cell adhesion models consider these parameters and can predict capture, rolling, and release events.

Shear stress

The local shear stress in a microfluidic device is a function of the device geometry, flow rate, and fluid properties. Both the maximum shear stress and the shear stress gradient can significantly impact viability as a cell traverses the device; existing devices have shear stresses ranging from 0–0.03 Pa and have captured CTCs [4, 5, 35] and endothelial progenitor cells [3] without significant decreases in viability. Shear-induced damage to cells simultaneously diminishes the population to be sampled and also contaminates any immunocoated surfaces with cell fragments. Therefore, the shear field and the geometry of surfaces with which target cells interact must be considered and assessed. Model systems, such as cell lines or polystyrene microspheres, provide insight, but anticipate only a subset of the physical issues of rare cell capture.

Immunospecificity

Immunocapture systems rely on the specificity of the ligand to a particular surface antigen. Key antigen considerations include specificity to a specific cell type or disease state, density and localization on the surface of the cell, and dependence of expression on confounding variables. In a device where blood is the target system to be processed, the nonspecific adhesion of leukocytes to surfaces can be substantial [4, 6]. Increased bond receptor– ligand bond strength improves the AUC of the ROC curve and enables purity to be increased by increasing local shear stress, within limits of viability.

Biorheology

The presence of the cells themselves leads to non-Newtonian behavior in whole blood, even though serum does not deviate from Newtonian behavior enough to affect most microfluidic systems. Several basic characteristics of biorheological flows are important for rare cell capture, including shear-induced diffusion, margination, and the Fahraeus effect. Shear-induced diffusion [36–39] describes the effective diffusion that particles in a dense suspension exhibit because particle–particle collisions in shear displace the particles, and this phenomenon is the primary source of diffusion for cells in whole blood (the native diffusion for cells is very small). Deformable particles near walls feel a lift force away from the surface, as a result of the shear gradient near the wall. At large particle densities and in complex mixtures of different cell types (e.g., in blood, where the hematocrit or volume fraction of cells is of the same order as the maximum packing fraction for spheres), stiffer cells tend to marginate, meaning that they move toward the walls [40], as shown in Figure 2. This process is not well understood and is typically attributed to many-body dynamics in blood. The Fahraeus effect describes the increase in particle volume fraction or hematocrit in small channels — this is attributable to particles being forced away from the walls, moving faster than the bulk solution, and therefore the suspension must have a smaller bulk fraction of particles to satisfy particle conservation. These mechanisms behind these effects are discussed in more detail in Section 3.

Adhesion models and reaction kinetics

Cell-adhesion models consider both the mechanical environment and the kinetics and thermodynamics involved in binding reactions [41, 42]. Within the receptor–ligand models, forward and reverse reaction rate coefficients, and thus an associativity coefficient, describe reaction kinetics [43]. Such models of reaction kinetics determine that these parameters are functions of local forcing, temperature, and receptor and ligand (and bond complex/transition state) lengths and material properties [43, 44]; many of these parameters are dependent on each other in various models.

Bond times and contact times affect the adhesion probabilities of cells on immunocoated surfaces [45]. The force experienced by cells results from a combination of the device geometry, fluid velocity and viscosity, and cell deformation and spreading, among other influences. Thus the sum of forces on the cell, in conjunction with bond type and flow rate, lead to differential modes of cell adhesion. As a cell adheres to an immunocoated surface, continued forcing with a prolonged residence time leads to continued bond formation (given receptors and ligands present) and greater adherence [45]. Given a short residence time, and high stresses or rapid velocities for the chemistry under consideration, a rolling event may ensue [45–47]. Continued motion is retarded by bonds tethering the cell to the surface; as the cell continues to experience for a torque and force as a consequence of the flow, it rolls about the point of adhesion. As cell motion overcomes the strength of the formed bond, the cell continues to move laterally, continually forming and breaking bonds, leading to detachment.

Numerical approaches for modeling these processes often include Brownian adhesive dynamics implemented via boundary element methods. In these techniques, forces are computed on deformable surfaces involving antibody–antigen pairs on the cell and surface by use of kinetic association and dissociation rates. Bond strengths are typically described with harmonic potentials and iterative generalized minimum residual solvers (GMRES) [48]. Periodic approximations at surfaces are often enhanced computationally by use of Ewald summation [49].

3 Cell transport in microfluidic devices

Cellular motion in microfluidic devices arises from the interaction of the cell with velocity, pressure, gravity, and electric fields. The velocity field (typically generated by an external pressure difference) advects the particle, which experiences pressure and viscous fluid stresses on its surface. The particle motion deviates from fluid motion owing to gravity, electrical fields, and particle–boundary interactions.

The Reynolds number, *Re*, characterizes the ratio of inertial and viscous forces,

$$Re=\frac{\rho U\ell}{\eta} \quad (1)$$

where ρ is the fluid density, U the characteristic velocity, ℓ a characteristic length scale, and η the dynamic viscocity. Recent work has employed moderate-to-high *Re* microdevices for rapid single-cell analysis [50], although most microfluidic systems for biological fluids result in length and velocity scales such that $Re \ll 1$. Known as Stokes flow, this regime is of practical importantance for cell capture devices, as the shear stresses are comparatively low; this review focuses exclusively on flow in low *Re* systems.

The significance of cell transport in a Stokes flow system is that the fluid, if the particles are dilute, prohibits a neutrally buoyant, rigid particle from crossing a streamline. Crossing of (or displacement onto adjacent) streamlines requires the particle to interact with a boundary (e.g., an obstacle) or be subject to forces exclusive of the fluid continuum (e.g., gravity, an electric field, or fluid microstructure). A key observation from this last point is that the particle trajectories within a device must be engineered to place cells in contact with the target structure; if this is not the case, another phenomena must be used to affect cell position. Many of these phenomena are always present in microfluidic devices, whereas others contribute such a small amount that they may be ignored. Batchelor [51] provides a thorough introduction to basic principles in fluid mechanics and Russel, et al. [52] describes important concepts of Stokes flow in detail. Here, we briefly discuss some of these phenomena, and then describe the transport phenomena behind some commonly used device platforms.

3.1 Diffusion

Diffusional transport occurs in all systems as a result of the random motion of molecules forced by the thermal energy. The concentration evolution as a function of time based on diffusion alone is

$$\frac{\partial c(\underline{r},t)}{\partial t}=D\nabla^2 c(\underline{r},t), \quad (2)$$

where D is the diffusivity, c the concentration, $\underline{r}$ the position vector, and t time. A similarity or Fourier integral transform solution or scale analysis yields a characteristic time $\tau_{diff} = \ell^2/D$ required for for a species to diffuse a length ℓ. This scaling is in contrast the convective motion of fluid, solutes, or cells, $\tau_{conv} = \ell/U$.

The ratio of the two transport timescales yields the mass transfer Péclet number, a parameter characterizing the dominant mode of transport

$$Pe \equiv \frac{\tau_{diff}}{\tau_{conv}}=\frac{U\ell}{D}. \quad (3)$$

The diffusivity of ions, molecules, cells, and particles can be approximated by the Stokes-Einstein relation,

$$D \frac{k_B T}{6\pi\eta a}. \quad (4)$$

Here, k_B is Boltzmann's constant, T is the temperature, and a the Stokes radius of the analyte. Table 1 provides a sampling of analytes, their diffusivites as calculated by the Stokes-Einstein relation, and a representative Péclet number at specific conditions. Importantly, the diffusivity of mammalian cells is extremely small, and the Péclet number is large for isolated cells in any microfluidic flow. Mammalian cells neither advect nor diffuse away from streamlines unless there is external forcing.

3.2 Deterministic cross-streamline motion

The previous analysis for convection considered inertialess flow without external forcing, in which case there is no motion across streamlines unless contact with a boundary occurs. Several additional cases are of interest: a system with non-negligible inertia, a system where the particles have density much different than that of the fluid, and a system where boundaries and fluid streams are introduced that strongly affect the nature of the particle motion — typically these effects leverage differences in particle size, although in some instances the electrical properties of cells are exploited.

Particle inertial effects—Given the flow, the Stokes number measures the tendency of the particle to deviate from the fluid streamline because its inertia resists acceleration; the Stokes number is a ratio of the particle time scale, τ_p and the flow time scale, τ_f. Typically, the particle time scale is taken as the force on the particle divided by the mass of the particle: $\tau_p = 2\rho_p a^2 / 9\mu$. The flow time scale depends on the physical characteristics of the flow, principally, how fast the flow varies. Using the length scale of an obstacle, r, divided by the average fluid velocity, U: $\tau_f = r / U$. For this case,

$$St = \frac{\tau_p}{\tau_f} = \frac{2\rho_p a^2 U}{9\mu r}. \quad (5)$$

In rare cell capture applications, the Stokes number is typically very small — the particle length scale is typically smaller or on the same order as the obstacle length scale (perhaps the characteristic length of an obstacle), and the densities of the plasma and cell are within 10%. In this case, a particle faithfully follows its fluid streamline.

Body forces—Cells can be actuated by gravity or electrical forces. When the particle density varies from that of the fluid, either flotation or sedimentation results. From the previous analysis, density affects the ability of the particle to trace fluid streamlines as well. However, particle motion due to density variations are mitigated by length scale and Reynolds number effects, so density variations are often not a cause of particle pathlines deviating from streamlines. Electrical fields generated by the presence of particles, boundaries between fluids, and externally applied potentials can lead to electrophoretic or dielectrophoretic forces as well.

Particle–wall interactions—Deformable cells or particles traveling along surfaces (for example, in long straight tubes) experience a force away from the surface — this force works against rare cell capture devices. Although this force is important in many applications, rare cell capture microdevices are typically designed to specifically avoid or

overwhelm this force, and a detailed description of this effect rarely plays a central role in describing device performance. In contrast, the displacement associated with cell–wall collisions and the downstream effect of these collisions is often a central factor.

As a particle travels along a streamline that approaches a solid boundary, its finite size prevents the particle center from moving closer than one particle radius (for a rigid spherical particle) to the boundary; more generally, deformable and nonspherical particles in general have a geometry- and rigidity-specific approach distance. Regardless of the details, the result is that the center of rare cells have a minimum distance from the surface; if the streamline on which a cell is traveling approaches the surface more closely than this distance, the resulting collision displaces the cell from the initial streamline and the cell pathline deviates from that streamline [6, 53–55].

4 Design strategies and applications in a transport context

The preceeding analysis shows that in the microdevice regime, particle trajectories are predominantly described by fluid streamlines. The Péclet number is typically very large and the Reynolds and Stokes numbers are both small. Collisions must be induced by structures that induce cell motion perpendicular to streamlines.

Rare cell capture at surfaces consists of a physical component: bringing as many rare cells as possible into contact with a surface (efficiency) and keeping most contaminating cells away from the wall (purity) — and a chemical component: ensuring that rare cells encountered by the surface are captured (efficiency) and that contaminating cells are not (purity). Thus the design of microfluidic devices can be split into the physical task of designing flows and geometries and the chemical task of designing surface functionalization schemes.

4.1 Designing flows and geometries

Near a straight, non-permeable wall, flow is parallel to the wall and motion along a streamline does not carry a cell to the wall. To bring cells in contact to a wall, we must either (a) depend on a diffusive process to cause cells to randomly move transverse to streamlines, (b) apply a body force (e.g., gravity or dielectrophoresis) to move the cells transverse to streamlines, (c) create geometries in the flow so that flow is accelerated, streamlines are compressed and the cells are effectively brought in proximity to the wall by motion along a streamline, or (d) make the wall permeable and allow the streamlines to cross the interface.

Diffusion length and surface-area-to-volume ratio—Diffusional movement of a cell to a wall is a governed by the Péclet number, which is a function of the cell's diffusivity and the length that the cell must travel. The highest rates of diffusion-drive cell–wall interactions are realized by minimizing the Péclet number and maximizing the surface-area-to-volume ratio; however, for most microchannels, even the smallest analytes have $Pe \gg 1$ (Table 1). Therefore, even in a limit where the surface-area-to-volume ratio is large, diffusion is insufficient to induce much cell–wall interaction. Increasing the surface area by shrinking the device improves performance for molecular analytes but still results in large Péclet number (low diffusion) flows for cells.

Velocity structures that fold or twist fluid streamtubes can shorten diffusion length scales by reducing the characteristic size of the fluid domains, demonstrated experimentally in Figure 3. These flow structures occur naturally in high-Re flows but are absent in many low-Re flows.

Chaotic advection is a term commonly used in the low-*Re* mixing literature [56–65]; in the context of cell motion toward a wall, chaotic advection uses the exponential deviation of trajectories to amplify a small random diffusive motion to a large effective motion. Thus a deterministic *fluid flow* can lead to a chaotic *cell trajectory* if the fluid flow amplifies the random aspect of the cellular diffusion. The characteristic length scale for chaotic advection scales as ln(*Pe*), but diffusion in these systems is limited by nonchaotic flow near the wall, which scales as $Pe^{1/4}$. In either case, the diffusion times are reduced; this will increase capture efficiency if *Pe* is modest, but will have no appreciable effect if *Pe* remains large.

Body forces—Body forces can be used to bring cells into contact with walls, especially in dilute suspensions, where cells are free to move without significant particle–particle interactions. Gravitational forces result in settling when there is a density difference between a cell and its surrounding media; capture efficiency and purity can be enhanced if density or size is specific to the rare cell phenotype. Gravity is commonly used to separate blood cells from each other and plasma using gradient centrifugation [66], but it is difficult to implement in a microfluidic device, where gravitational acceleration would be limited to 1 *g* and particle–particle interactions in whole blood result in comparatively slow settling velocities.

Dielectrophoresis (DEP) results from particle polarization in a nonuniform electric field and can be used to actuate cells in blood [67]. A cell's DEP response is a function of the properties of the cell membrane and the cytoplasm [68]. Depending on a cell's polarizibility relative to the surrounding media, it may be attracted to stronger electric field regions (positive DEP) or repelled (negative DEP) [1]. Positive DEP can be used to trap a cell; negative DEP can be combined with a nonuniform velocity field such that particles have different elution times based on their DEP response (DEP field-flow fractionation) [67]. DEP is difficult to implement in practice, however, as it typically requires that cells be diluted in a buffer of controlled osmolarity and conductivity so that rare cells and blood cells are actuated differently.

Obstacles—In the presence of bluff-body obstacles, diffusion is not required for cells to come into contact with the surface — rather, the presence of the obstacles deflects the fluid flow, inducing flow deceleration and streamline dilatation (at the front and rear surfaces of the obstacle) with flow acceleration and streamline compression (at the shoulders of the obstacle). The compression of streamlines brings cells into proximity with the surface as the cells progress along a streamline. The presence of obstacles, independent of their orientation with respect to each other, enhances the collisions of particles, increasing the capture efficiency, for example, of circulating tumor cells captured from blood [4, 6, 25]. Although adding obstacles to a cell-capture system does enhance the surface-area-to-volume ratio, the Péclet number is too large for the surface-area-to-volume ratio to matter — it is the deceleration at the upstream edge and the streamline compression at the shoulder that enhance cell capture efficiency, not the reduction in characteristic diffusion length.

Obstacle *arrays* have several properties that lend themselves to microfluidic cell transport applications. The rational array geometry, shown in Figure 5, lends itself to parametric engineering design studies, and can be optimized to control particle motion [54, 69] and particle– obstacle collision dynamics [6]. Such obstacle arrays are easy to fabricate with standard photolithography techniques, and can be readily integrated into up- and downstream devices. The large number of obstacles in the array results in a system that is robust to local flow disruptions caused by fabrication errors and inlet and outlet conditions.

Obstacle arrays are notable in that they afford a physical means for enhancing capture *purity* in addition to capture *efficiency*. The distortion of streamlines and the deflection particles

experience upon contact with obstacles leads both to enhanced capture (if the surface is functionalized with an appropriate antibody) and, when capture does not occur, to deflection and transverse displacement of particles. In obstacle arrays with no surface functionalization, the deflection of particles has been shown to be size dependent [53–55], as the streamline experienced by the particle center when in contact with an obstacle is dependent on the size of the particle. Thus the streamline dilatation on the downstream face of the obstacle leads to size-dependent particle separation, which then leads to size-dependent trajectories as the particle separation causes particles to collide with different sides of obstacles in the following rows. This phenomenon has at times been termed *deterministic lateral displacement*, to contrast with diffusionally-driven size-based separation processes. Similar ideas have been used for spatial particle separation; termed *pinched-flow fractionation*, this technique uses the junction of two flows to press particles up against a surface before a streamline expansion separates them [70]. Spatial separation of cells based on size alone is often of limited use in rare cell capture from blood — although rare cells and particles can be smaller (virions) or larger (erythroblasts, CTCs) on average than hematological cells, the sizes of rare cells has a broad distribution, and size is often much less specific to the rare cell phenotype than surface markers specified by immunocoated surfaces. If size-dependent cell trajectories are combined with immunocoated surfaces, the observed cell efficiency and purity are both improved [6]; this approach has been termed geometrically enhanced differential immunocapture (GEDI). Figure 6 shows collision frequency as a function of particle size in an example GEDI geometry [25], highlighting the typical sharp transition between low and high collision frequency.

Porous boundaries—Cell transport towards solid boundaries is inherently limited by the nopenetration velocity condition at the boundary's surface; streamlines near the boundary run parallel to it. One simple solution to enhance motion normal to the surface is to use porous walls combined with a transverse pressure gradient. This results in target particles being pulled toward the wall as the carrier fluid flows out of the channel [71]. Unlike porous filter-based microdevices [72], particles are not trapped, but adhesion can be enhanced by direct contact and a pressure-induced normal force.

4.2 Controlling particle adhesion

Having discussed geometries that bring rare cells into contact with an immunofunctionalized surface, we turn our attention to the chemical task of designing surface functionalization schemes. Successful capture requires an antigen present in large numbers on the surface of the cell, an antibody specific to that antigen, and a strong antibody–antigen avidity. In addition, the two binding sites must be spatially accessible to one another.

Once a cell comes into contact with the capture surface, the number and avidity of potential antigen-antibody binding sites are key to overcoming fluid forces that would otherwise dislodge the cell. For a specific antibody-antigen pair, the capture efficiency decreases with increasing shear stress [35], as demonstrated in Figure 7.

The location of potential binding sites on the antibody and antigen are key to successful capture. Regardless of binding affinities, both binding sites must be sterically accessible to each other such that the bond can form. As an example, two antibodies specific to PSMA, biotinylated-J415 and -J591, have similar chemical affinities [73] but J415's binding site is located near the transmembrane domain of the protein, while J591's binding site is located at the apical domain. As such, steric repulsion makes it less likely that a wall-bound J415 antibody will bind with a target cell's PSMA than a J591 antibody. This distinction is present only under flow and is not evident in an immunofluorescent experiment. Figure 7

shows the net result of this steric interaction; J591 outperforms J415 in the capture of LNCaP prostate cancer cells [35].

5 Concluding remarks

The performance of rare cell capture devices, as measured by capture efficiency and sample purity, is primarily affected by two phenomena: the chemical interaction between the cell and the capture surface and the transport of cells to (and their collision dynamics with) the capture surface. Modern rare cell immunocapture devices use both chemical and fluid-dynamic optimization to maximize the efficiency and purity of capture.

Extracellular surface markers specific to the target cell enable capture of the target cell and reject contaminating populations. Adhesion models consider the mechanical environment, the kinetics of bond complexes resulting in receptor–ligand interactions, the thermodynamics of the binding reactions, and the steric effects of antigen location relative to a device wall. Most importantly, the interplay between fluid forces and adhesion can be optimized to reduce the effect of nonspecific adhesion with respect to the specific targeted adhesion caused by an immunocoated surface.

Flow near surfaces induces few cell–wall collision when the no-penetration condition is satisfied; this boundary condition limits collision frequency but provides opportunities to optimize performance by using the fluid mechanics to enhance purity based on mechanical properties of the cells. Porous surfaces with finite penetration tend to maximize capture efficiency but do not add a fluid-specific purification.

Mechanical property variation, most importantly size differences between target- and non-target cells, can be leveraged to create size-dependent transport and collision dynamics. Because steric interactions with surfaces are often the dominant source of cell motion across streamlines, bluff-body obstacles are simultaneously the simplest way to induce collision and generate size-dependent transport across streamlines. In some systems, size-dependent transport can be used to increase purity and therefore enhance overall system receiver–operator characteristics.

Acknowledgments

This work was supported by the Cornell Center on the Microenvironment & Metastasis through Award Number U54CA143876 from the National Cancer Institute.

Abbreviations

AUC	area under curve
CD*n*	cluster of differentiation *n*
CTC	circulating tumor cell
EGFR	epidermal growth factor receptor
EpCAM	epithelial cell adhesion molecule
FFF	field-flow fractionation
GEDI	geometrically enhanced differential immunocapture
HER2	human epidermal growth factor receptor 2
MUC*n*	mucin-*n*

PSMA	prostate-specific membrane antigen
RNA	ribonucleic acid
ROC curve	receiver operating characteristic curve
VEGFR	vascular endothelial growth factor receptor.

References

1. Pratt ED, Huang C, Hawkins BG, Gleghorn JP, Kirby BJ. Chem. Eng. Sci. 2011; 66:1508–1522. [PubMed: 21532971]
2. Cheng X, Irimia D, Dixon M, Sekine K, Demirci U, Zamir L, Tompkins RG, Rodriguez W, Toner M. Lab Chip. 2007; 7:170–178. [PubMed: 17268618]
3. Hatch A, Hansmann G, Murthy SK. Langmuir. 2011; 27:4257–4264. [PubMed: 21401041]
4. Nagrath S, Sequist LV, Maheswaran S, Bell DW, Irimia D, Ulkus L, Smith M, Kwak EL, Digurmarthy S, Muzikansky A, Ryan P, Balis U, Tompkins RG, Haber DA, Toner M. Nature. 2007; 450:1235–1239. [PubMed: 18097410]
5. Stott SL, Lee RJ, Nagrath S, Yu M, Miyamoto DT, Ulkus L, Inserra EJ, Ulman M, Springer S, Nakamura Z, Moore AL, Tsukrov DI, Kempner ME, Dahl DM, Wu C-L, Iafrate AJ, Smith MR, Tompkins RG, Sequist LV, Toner M, Haber DA, Maheswara S. Sci. Trans. Med. 2010
6. Gleghorn JP, Pratt ED, Denning D, Liu H, Bander NH, Tagawa ST, Nanus DM, Giannakakou PA, Kirby BJ. Lab Chip. 2010; 10:27–29. [PubMed: 20024046]
7. Hsieh HB, Marrinucci D, Bethel K, Curry DN, Humphrey M, Krivacic RT, Kroener J, Kroener L, Ladanyi A, Lazarus N, Kuhn P, Bruce RH, Nieva J. Biosens. Bioelectron. 2006; 21:1893–1899. [PubMed: 16464570]
8. Talasaz AH, Powell AA, Huber DE, Berbee JG, Roh K-H, Yu W, Xiao W, Davis MM, Pease RF, Mindrinos MN, Jeffrey SS, Davis RW. Proc. Natl. Acad. Sci. USA. 2009; 106:3970–3975. [PubMed: 19234122]
9. Laerum OD, Farsund T. Cytometry. 1981; 2:1–13. [PubMed: 7023887]
10. Morgan AC, Schroff RW, Ortaldo JR, Herberman RB. J. Clin. Lab. Anal. 1988; 2:182–186.
11. Givan, A. Flow cytometry: First principles. Wiley-Liss; 1992.
12. Shapiro, H. Practical Flow Cytometry. Wiley-Liss; 2003.
13. Chaudry MA, Sales K, Ruf P, Lindhofer H, Winslet MC. Br. J. Cancer. 2007; 96:1013–1019. [PubMed: 17325709]
14. Kuroda K, Liu H, Kim S, Guo M, Navarro V, Bander NH. Prostate. 2009; 69:1579–1585. [PubMed: 19575420]
15. Tagawa ST, Beltran H, Vallabhajosula S, Goldsmith SJ, Osborne J, Matulich D, Petrillo K, Parmar S, Nanus DM, Bander NH. Cancer. 2010; 116:1075–1083. [PubMed: 20127956]
16. Rainusso N, Man TK, Lau CC, Hicks J, Shen JJ, Yu A, Wang LL, Rosen JM. Cancer Biol. Ther. 2011; 12:278–287. [PubMed: 21617384]
17. Rao C, Chianese D, Doyle G, Miller C, Russell T, Sanders R, Terstappen L. Int. J. Oncol. 2005; 27:46–57.
18. Sieuwerts AM, Kraan J, Bolt J, van der Spoel P, Elstrodt F, Schutte M, Martens JWM, Gratama J-W, Sleijfer S, Foekens JA. J. Natl. Cancer Inst. 2009; 101:61–66. [PubMed: 19116383]
19. Stimpfl M, Schmid BC, Schiebel I, Tong D, Leodolter S, Obermair A, Zeillinger R. Cancer Lett. 1999; 145:133–141. [PubMed: 10530781]
20. Qu CF, Li Y, Song YJ, Rizvi SMA, Raja C, Zhang D, Samra J, Smith R, Perkins AC, Apostolidis C, Allen BJ. Br. J. Cancer. 2004; 91:2086–2093. [PubMed: 15599383]
21. Saitou M, Goto M, Horinouchi M, Tamada S, Nagata K, Hamada T, Osako M, Takao S, Batra S, Aikou T, Imai K, Yonezawa S. J. Clin. Path. 2005; 58:845–852. [PubMed: 16049287]
22. Hattrup CL, Gendler SJ. Annu. Rev. Physiol. 2008; 70:431–457. [PubMed: 17850209]
23. Reid A, Vidal L, Shaw H, de Bono J. Eur. J. Cancer. 2007; 43:481–489. [PubMed: 17208435]

24. Perner S, Hofer MD, Kim R, Shah RB, Li H, Mˆller P, Hautmann RE, Gschwend JE, Kuefer R, Rubin MA. Hum. Pathol. 2007; 38:696–701. [PubMed: 17320151]
25. Kirby BJ, Jodari M, Loftus MS, Gakhar G, Pratt ED, Chanel-Vos C, Gleghorn JP, Santana SM, Liu H, Smith JP, Navarro VN, Tagawa ST, Bander NH, Nanus DM, Giannakakou P. PLoS ONE. 2012; 7:e35976. [PubMed: 22558290]
26. Jain S, Ward M, O'Loughlin J, Boeck M, Wiener N, Chuang E, Cigler T, Moore A, Donovan D, Lam C, Cobham M, Schneider S, Christos P, Baergen R, Swistel A, Lane M, Mittal V, Rafii S, Vahdat L. Breast Cancer Res. Treat. 2012; 132:235–242. [PubMed: 22160642]
27. Fung, Y. Biomechanics: Mechanical Properties of Living Tissues. Springer; 2004.
28. Zheng S, Lin H, Liu J-Q, Balic M, Datar R, Cote RJ, Tai Y-C. J. Chromatogr. A. 2007; 1162:154–161. [PubMed: 17561026]
29. Mathivanan S, Ji H, Simpson RJ. J. Proteomics. 2010; 73:1907–1920. [PubMed: 20601276]
30. Camussi G, Deregibus MC, Bruno S, Grange C, Fonsato V, Tetta C. Amer. J. Cancer Res. 2011; 1:98–110. [PubMed: 21969178]
31. Cristofanilli M, Budd GT, Ellis MJ, Stopeck A, Matera J, Miller MC, Reuben JM, Doyle GV, Allard WJ, Terstappen LW, Hayes DF. N. Engl J. Med. 2004; 351:781–791. [PubMed: 15317891]
32. Racila E, Euhus D, Weiss AJ, Rao C, McConnell J, Terstappen LWMM, Uhr JW. Proc. Natl. Acad. Sci. USA. 1998; 95:4589–4594. [PubMed: 9539782]
33. Marrinucci D, Bethel K, Lazar D, Fisher J, Huynh E, Clark P, Bruce R, Nieva J, Kuhn P. J. Oncol. 2010
34. Tomlins SA, Rhodes DR, Perner S, Dhanasekaran SM, Mehra R, Sun X-W, Varambally S, Cao X, Tchinda J, Kuefer R, Lee C, Montie JE, Shah RB, Pienta KJ, Rubin MA, Chinnaiyan AM. Science. 2005; 310:644–648. [PubMed: 16254181]
35. Santana SM, Liu H, Bander NH, Gleghorn JP, Kirby BJ. Biomed. Microdevices. 2012; 14:401–407. [PubMed: 22143878]
36. Leighton D, Acrivos A. J. Fluid Mech. 1987; 177:109–131.
37. Acrivos A, Batchelor GK, Hinch EJ, Koch DL, Mauri R. J. Fluid Mech. 1992; 240:651–657.
38. Acrivos A. J. Rheol. 1995; 39:813–826.
39. Wang Y, Mauri R, Acrivos A. J. Fluid Mech. 1998; 357:279–287.
40. Zhao H, Shaqfeh ESG. Phys. Rev. E. 2011; 83 061924.
41. Zhu C, Bao G, Wang N. Ann. Rev. Biomed. Eng. 2000; 2:189. [PubMed: 11701511]
42. Dustin ML, Ferguson LM, Chan PY, Springer TA, Golan DE. J. Cell Biol. 1996; 132:465–74. [PubMed: 8636222]
43. Bell GI, Dembo M, Bongrand P. Biophys. J. 1984; 45:1051–1064. [PubMed: 6743742]
44. Dembo M, Torney DC, Saxman K, Hammer D. 1988; 234:55–83.
45. Dong C, Lei XX. J. Biomech. 2000; 33:35–43. [PubMed: 10609516]
46. Lawrence MB, Springer TA. Cell. 1991; 65:859–873. [PubMed: 1710173]
47. Alon R, Hammer DA, Springer TA. Nature. 1995; 374:539–542. [PubMed: 7535385]
48. Saad Y, Schultz MH. SIAM J. Sci. Stat. Comp. 1986; 7:856–869.
49. Saintillan D, Darve E, Shaqfeh ESG. Phys. Fluids. 2005; 17 033301.
50. Carlo DD. Lab Chip. 2009; 9:3038–3046. [PubMed: 19823716]
51. Batchelor, GK. An Introduction to Fluid Dynamics. Cambridge: 1967.
52. Russel, WB.; Saville, DA.; Schowalter, WR. Colloidal Dispersions. Cambridge: 1989.
53. Huang LR, Cox EC, Austin RH, Sturm JC. Science. 2004; 304:987–990. [PubMed: 15143275]
54. Inglis D, Davis J, Austin R, Sturm J. Lab Chip. 2006; 6:655–658. [PubMed: 16652181]
55. Long BR, Heller M, Beech JP, Linke H, Bruus H, Tegenfeldt JO. Phys. Rev. E. 2008; 78 046304.
56. Ottino, JM. The Kinematics of Mixing: Stretching, Chaos, and Transport. Cambridge: 1989.
57. Liu R, Stremler M, Sharp K, Olsen M, Santiago J, Adrian R, Aref H, Beebe D. J. Microelectromech. S. 2000; 9:190–197.
58. Song H, Bringer MR, Tice JD, Gerdts CJ, Ismagilov RF. Appl. Phys. Lett. 2003; 83:4664–4666. [PubMed: 17940580]

59. Stroock AD, Dertinger SKW, Ajdari A, Mezi*fá* I, Stone HA, Whitesides GM. Science. 2002; 295:647–651. [PubMed: 11809963]
60. Raynal F, Plaza F, Beuf A, Carrière P, Souteyrand E, Martin J-R, Cloarec J-P, Cabrera M. Phys. Fluids. 2004; 16:L63–L66.
61. McQuain MK, Seale K, Peek J, Fisher TS, Levy S, Stremler MA, Haselton FR. Anal. Biochem. 2004; 325:215–226. [PubMed: 14751256]
62. Simonnet C, Groisman A. Phys. Rev. Lett. 2005; 94:134501. [PubMed: 15903994]
63. Wei C-W, Cheng J-Y, Huang C-T, Yen M-H, Young T-H. Nucleic Acids Res. 2005; 33:e78. [PubMed: 15891111]
64. Stremler M, Cola B. Phys. Fluids. 2006; 18
65. Hertzsch J-M, Sturman R, Wiggins S. Small. 2007; 3:202–218. [PubMed: 17262763]
66. English D, Andersen BR. J. Immunolog. Meth. 1974; 5:249–252.
67. Gascoyne PRC, Noshari J, Anderson TJ, Becker FF. Electrophoresis. 2009; 30:1388–1398. [PubMed: 19306266]
68. Kirby, BJ. Micro- And Nanoscale Fluid Mechanics: Transport in Microfluidic Devices. Cambridge: 2010.
69. Davis J, Inglis D, Morton K, Lawrence D, Huang L, Chou S, Sturm J, Austin R. Proc. Natl. Acad. Sci. USA. 2006; 103:14779–14784. [PubMed: 17001005]
70. Yamada M, Nakashima M, Seki M. Anal. Chem. 2004; 76:5465–5471. [PubMed: 15362908]
71. Chen GD, Fachin F, Fernandez-Suarez M, Wardle BL, Toner M. Small. 2011; 7:1061–1067. [PubMed: 21413145]
72. Lin HK, Zheng S, Williams AJ, Balic M, Groshen S, Scher HI, Fleisher M, Stadler W, Datar RH, Tai Y-C, Cote RJ. Clin. Cancer Res. 2010
73. Smith-Jones PM, Vallabahajosula S, Goldsmith SJ, Navarro V, Hunter CJ, Bastidas D, Bander NH. Cancer Res. 2000; 60:5237–5243. [PubMed: 11016653]

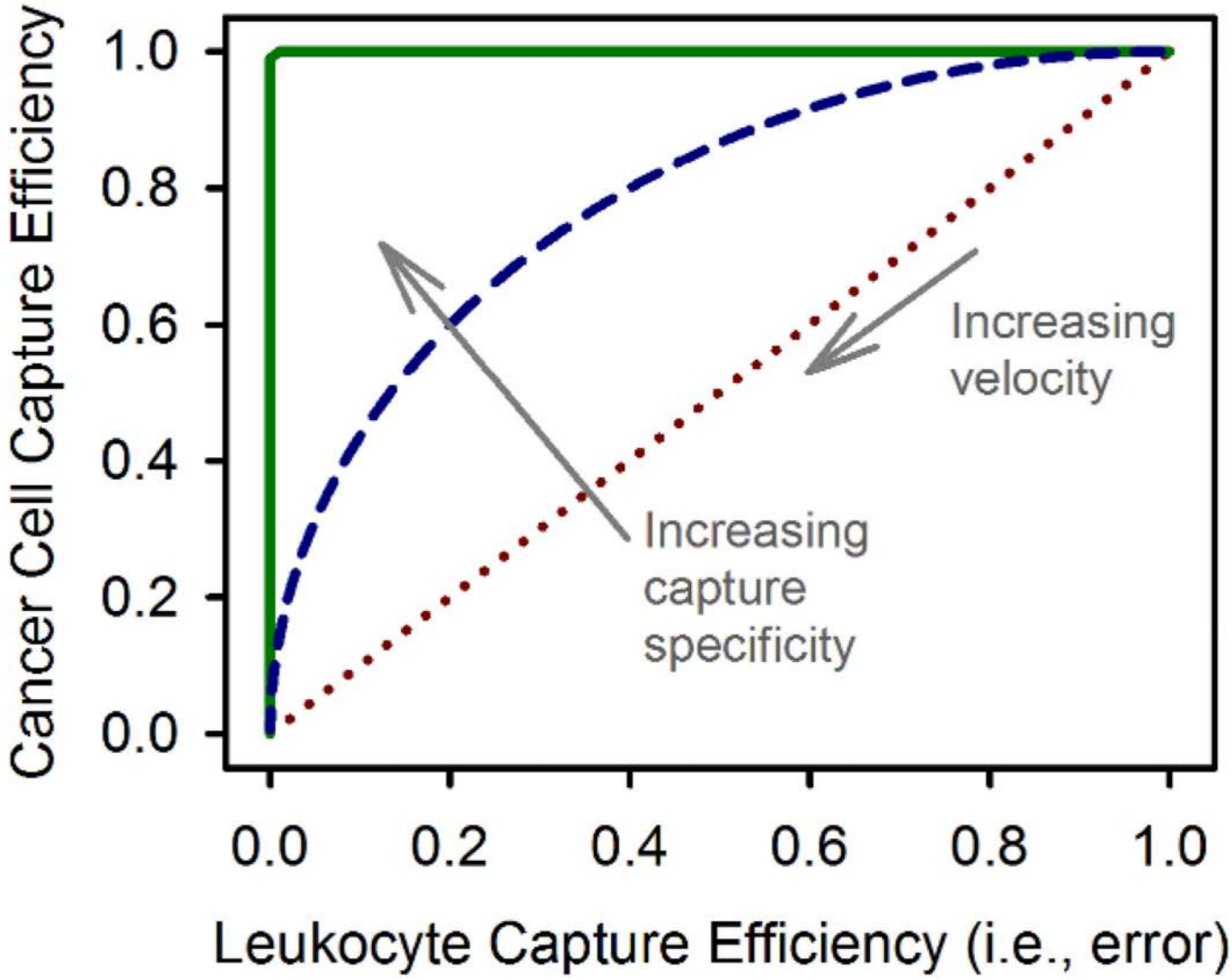

Figure 1.

An example of a receiver operating characteristic (ROC) curve, which shows the sensitivity of a rare cell capture device; in this example we consider only cancer cell capture versus capture of leukocytes, the most common contaminant. A given geometry, antibody, and velocity results in a balance between cancer cell capture efficiency (true positives) and leukocyte capture efficiency (false positives). A practical device (blue dashes) has an ROC curve between pure chance (red dots) and a theoretical perfect test (green line).

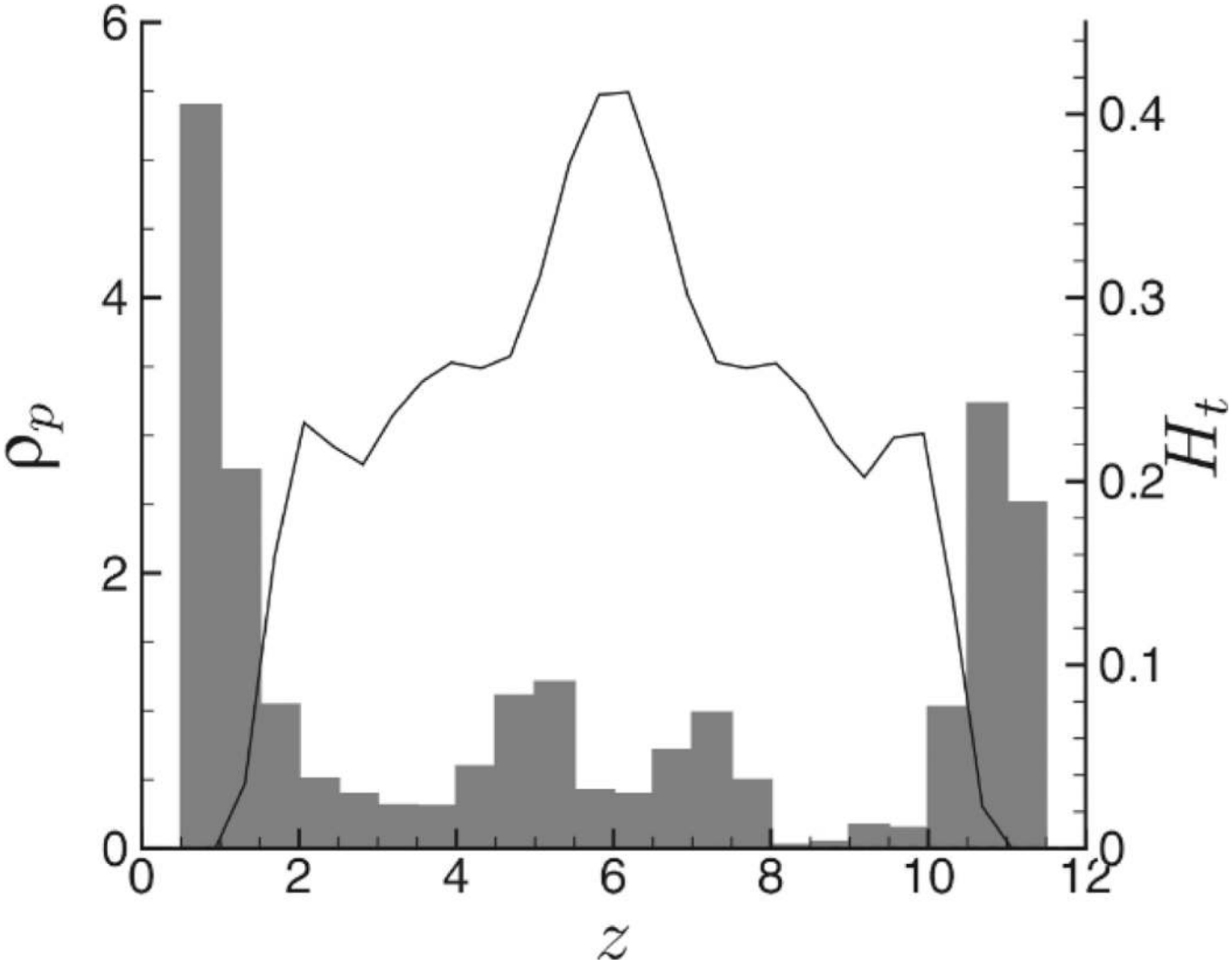

Figure 2.
Margination causes increased platelet density (ϱ_p, shaded bars) at the walls (z=0 and 12, respectively), while erythrocytes are concentrated in the center of the channel, as measured by the blood hematocrit (H_t, solid line). Adapted from [40].

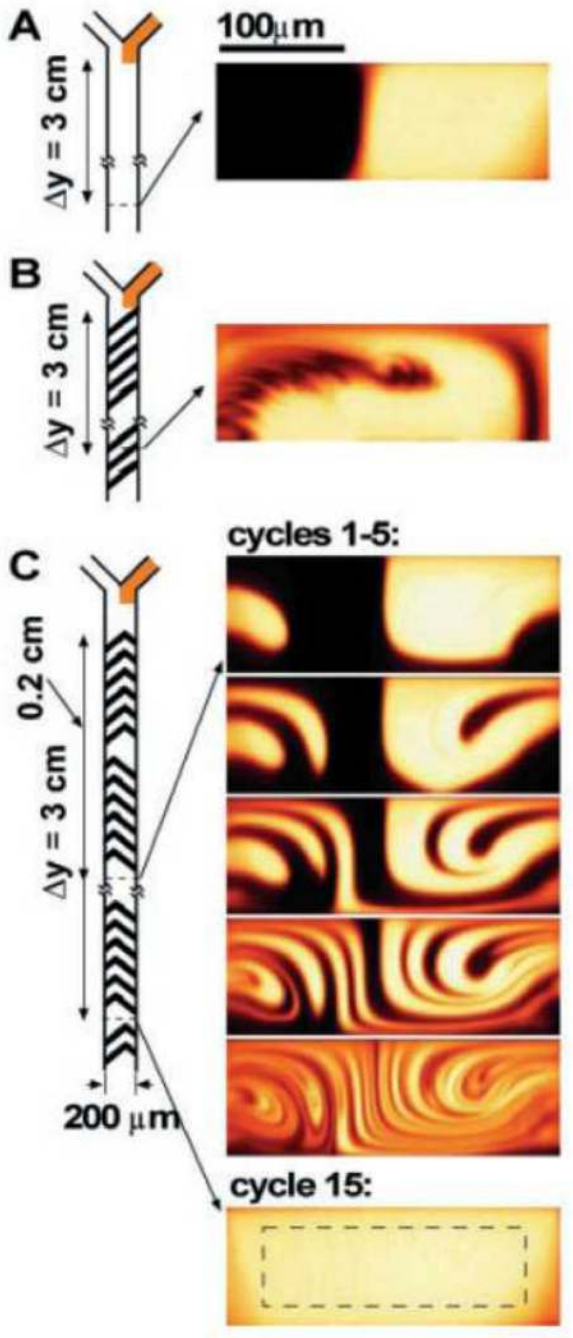

Figure 3.
Cross sections of the dye distribution in a microfluidic channel designed to create staggered, time-dependent whorls or twist maps. From [59]; used with permission.

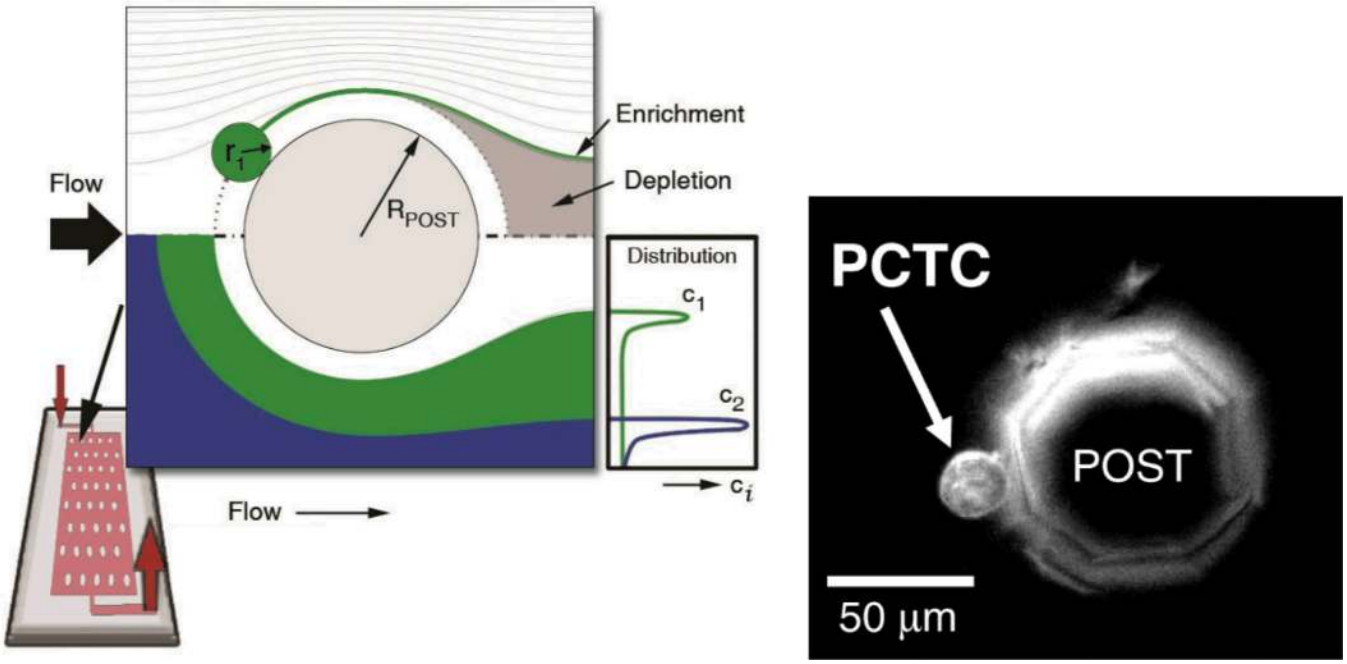

Figure 4.
Distribution of two populations of particles approaching a circular obstacle. Local streamline distortion enhances the collision of particles with the obstacle, increasing efficiency in cell-capture systems (left). A prostate circulating tumor cell (PCTC) captured on a octagonal obstacle post (right) [6].

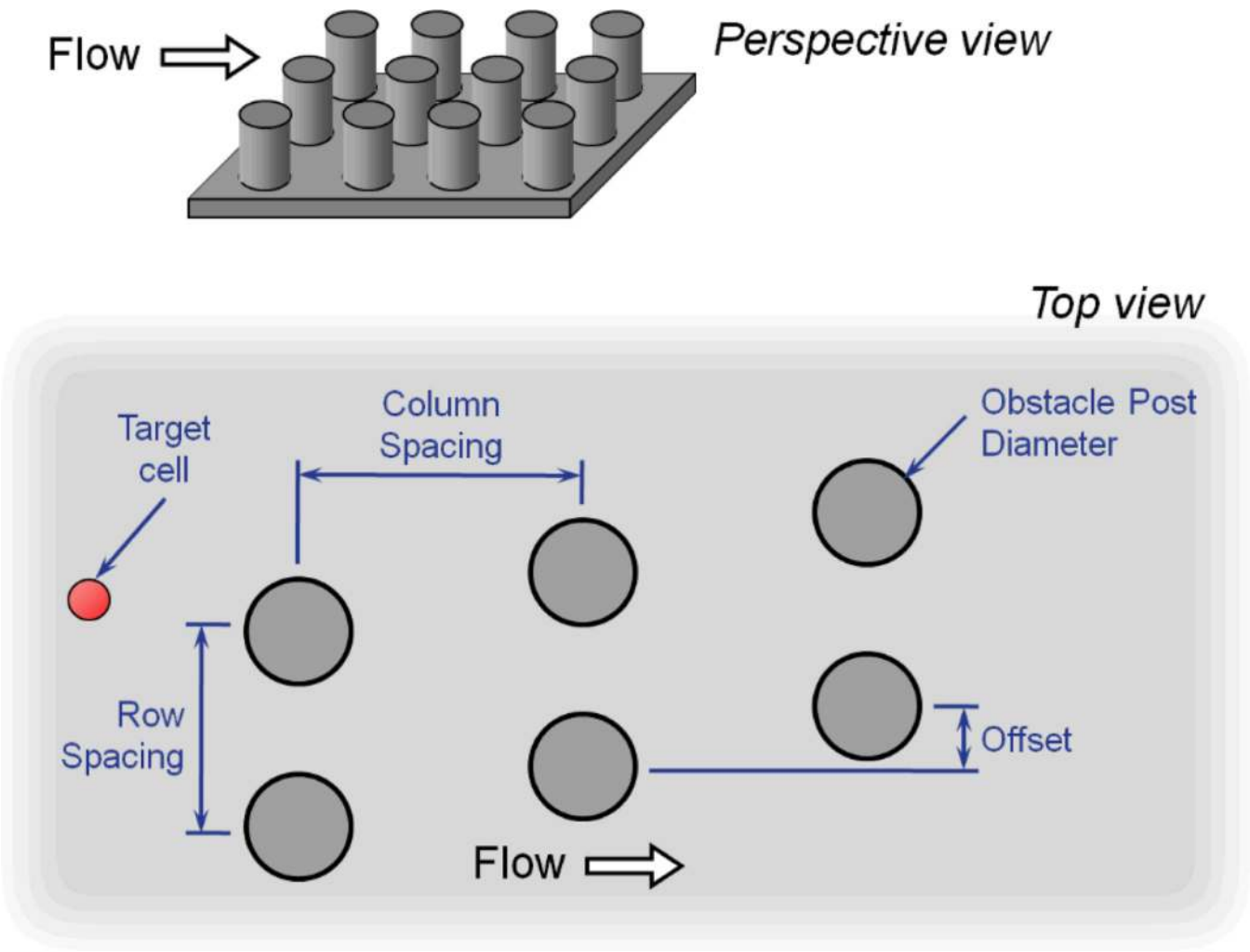

Figure 5.
An obstacle array's rational geometry lends itself to parametric engineering optimization.

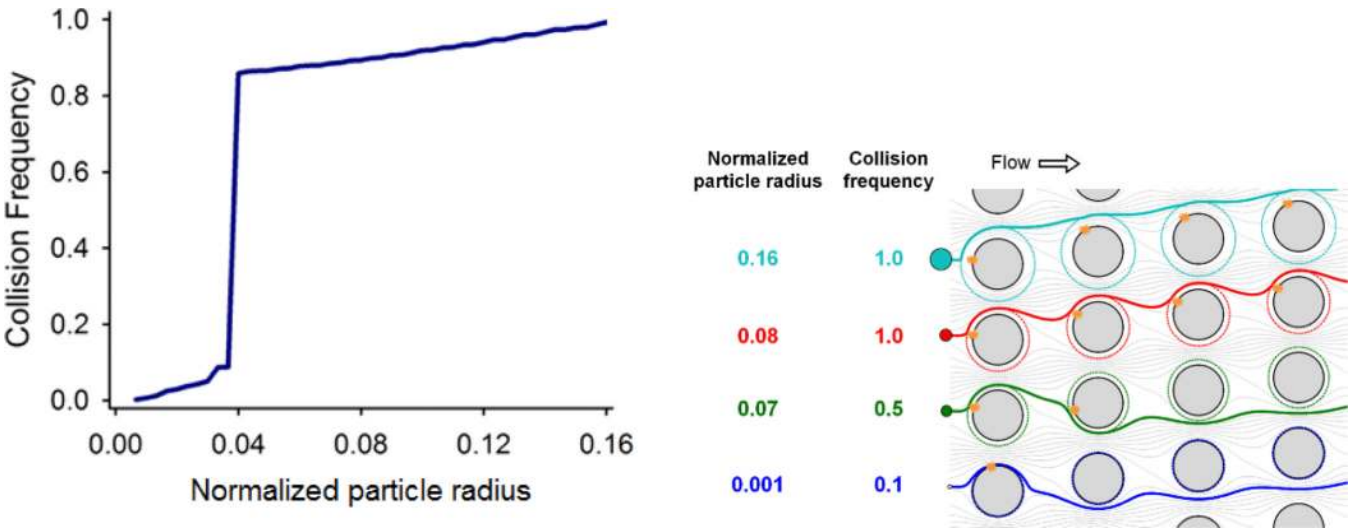

Figure 6.

Collision frequency versus particle size in a GEDI obstacle array (left). The sharp transition between high and low collision frequencies is also made evident by comparing particle trajectories (right). Size-dependent collision dynamics, combined with a specific immunocoated surface, maximize both efficiency and purity.

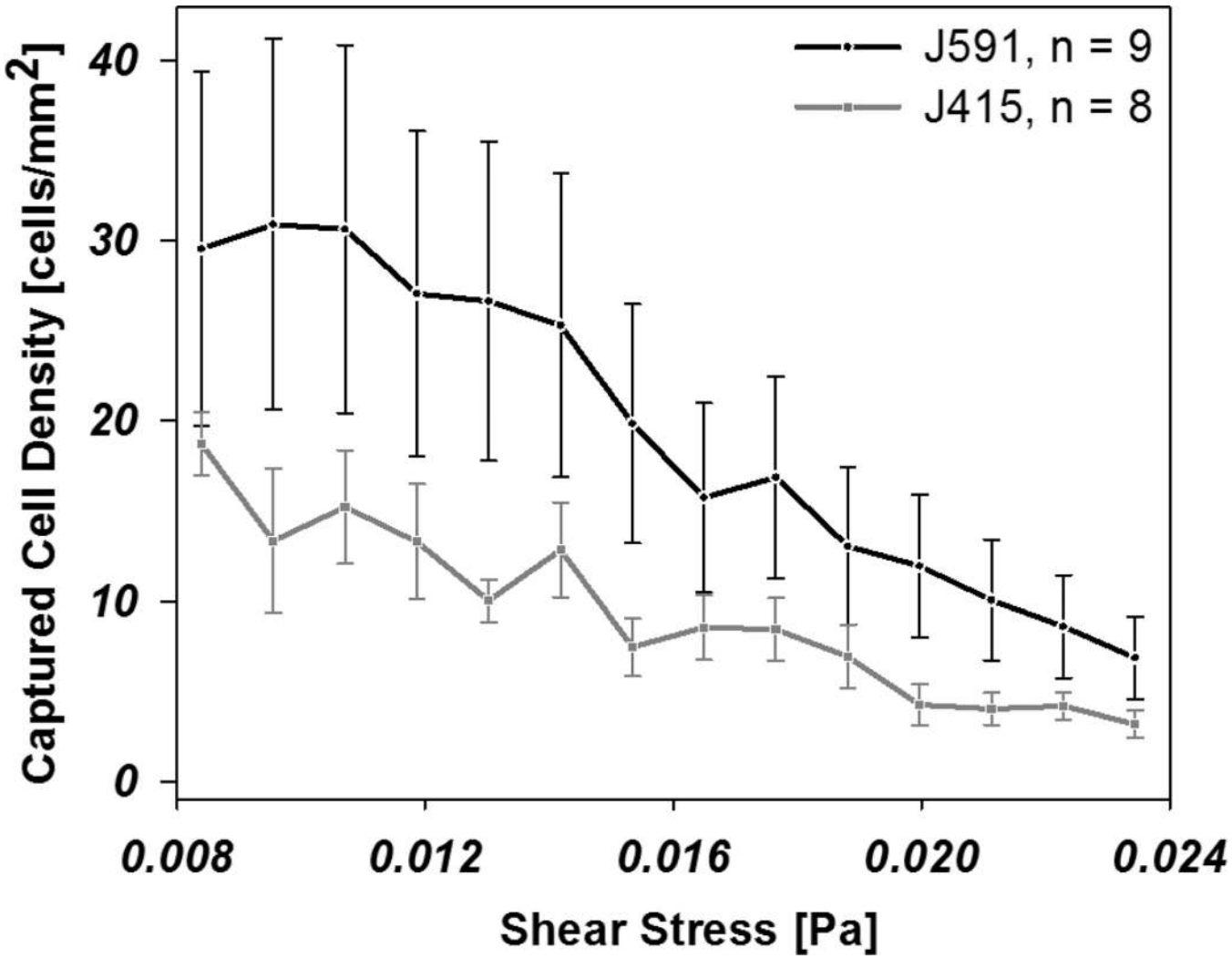

Figure 7.
LNCaP cell capture rates as a function of shear stress and capture surface immunochemistry. J415 and J591 have similar affinities [73] but differences in binding site location result in J591 (located at the protein's apical domain) outperforming J415 (located near the transmembrane domain). Adapted from [35], with permission.

Table 1

Diffusivities and representative Péclet numbers for dilute analytes in water at 25°C. Diffusivities were calculated with equation (4); Péclet numbers assume a 100 μm wide channel and 100 μm/s mean velocity.

Analyte	D (m^2/s)	*Pe*
Na^+, 100 pm	10^{-9}	10
BSA, 100 Å	10^{-11}	10^3
Viron, 100 nm	10^{-12}	10^4
Bacterial cell, 1 μm	10^{-13}	10^5
Erythrocyte, 10 μm	10^{-14}	10^6
Polystyrene bead, 100 μm	10^{-15}	10^7